JOURNAL OF CATALYSIS **172,** 222–237 (1997)
ARTICLE NO. CA971870

In-Situ Infrared Study of Methanol Synthesis from H_2/CO_2 over Cu/SiO_2 and $Cu/ZrO_2/SiO_2$

Ian A. Fisher and Alexis T. Bell

Chemical Sciences Division, Lawrence Berkeley National Laboratory and Department of Chemical Engineering, University of California, Berkeley, California 94720-1462

Received June 11, 1997; revised August 12, 1997; accepted August 14, 1997

The interactions of CO_2 and H_2/CO_2 with Cu/SiO_2, ZrO_2/SiO_2, and $Cu/ZrO_2/SiO_2$ have been investigated by *in-situ* infrared spectroscopy with the aim of understanding the nature of the species involved in methanol synthesis and the dynamics of the formation and consumption of these species. In the case of Cu/SiO_2, the only species observed during methanol synthesis are formate groups on Cu and methoxide groups on silica. When ZrO_2/SiO_2 or $Cu/ZrO_2/SiO_2$ is exposed to H_2/CO_2 the majority of the species observed are associated with ZrO_2. CO_2 adsorption on either ZrO_2/SiO_2 or $Cu/ZrO_2/SiO_2$ leads to the appearance of carbonate and bicarbonate species on the surface of ZrO_2. In the presence of H_2 these species are converted to formate and then methoxide species adsorbed on ZrO_2. The presence of Cu greatly accelerates the hydrogenation of bicarbonate to formate species, and the hydrogenation of formate to methoxide species. On $Cu/ZrO_2/SiO_2$ methylenebisoxy species are observed as intermediates in the latter reaction. While Cu promotes the reductive elimination of methoxide species as methanol, it is observed that hydrolytic release of methoxide species from ZrO_2 occurs much more rapidly than reductive elimination. Thus, the methanol synthesis over $Cu/ZrO_2/SiO_2$ is envisioned to occur on ZrO_2, with the primary role of Cu being the dissociative adsorption of H_2. The spillover of atomic H onto ZrO_2 provides the source of hydrogen needed to hydrogenate the carbon-containing species. It is also proposed that the formation of CO via the reverse-water–gas-shift reaction occurs on Cu.

INTRODUCTION

The industrial importance of methanol has resulted in significant research regarding its catalytic synthesis from hydrogen, carbon monoxide, and carbon dioxide. As methanol synthesis is an exothermic process, the equilibrium yield declines with increasing temperature. For this reason, efforts have been undertaken to enhance the activity of methanol synthesis catalysts, so that they may be operated at lower temperatures. Supported Cu catalysts have received much attention. Although some authors have shown the role of the support in methanol synthesis is minimal (1, 2), other studies have shown that the support or promoter can significantly affect the activity for methanol synthesis (3–5). Zirconia has emerged as a particularly interesting support material, as it enhances the activity of Cu for methanol synthesis from both CO/H_2 and CO_2/H_2 (4, 6–16). Although several studies have confirmed the promotional effect of zirconia on the activity of Cu, studies of the surface species formed under reaction conditions are less extensive (17–19). These studies have shown that zirconia provides adsorption sites for the reactive intermediates and suggest that adsorbed CO is reduced to methanol via a formaldehyde intermediate.

In the present study the interactions of CO_2 and H_2/CO_2 with Cu/SiO_2, ZrO_2/SiO_2, and $Cu/ZrO_2/SiO_2$ at elevated pressure were investigated by *in-situ* FTIR spectroscopy. This work was undertaken to provide further insight into the nature of the surface species present under reaction conditions and their relationship to the mechanism of methanol synthesis. Previous work (16) has shown that the presence of zirconia greatly enhances the rate of methanol synthesis, but it has a minimal effect on the reverse-water–gas-shift reaction rate. Therefore, it was also of interest to ascertain whether the behavior of the observable surface intermediates could be used to explain the reported trends in activity. Similar studies of the interaction of CO and H_2/CO are the subject of a forthcoming paper.

EXPERIMENTAL

The preparation and characterization of the Cu/SiO_2 and $Cu/ZrO_2/SiO_2$ catalysts used in this study have been described elsewhere (16). ZrO_2 was dispersed on SiO_2 in the same manner used to disperse ZrO_2 on Cu/SiO_2 (16). The Cu and Zr contents of the catalysts were determined by X-ray fluorescence analysis. The Cu surface areas of the catalysts were determined by N_2O titration (16). By these methods, the Cu/SiO_2 catalyst was determined to contain 5.7 wt% Cu with a Cu surface area of 1.36 m^2 per gram of catalyst (3.7% Cu dispersion); the ZrO_2/SiO_2 catalyst contained 32.6 wt% ZrO_2; and the $Cu/ZrO_2/SiO_2$ catalyst contained 5.7 wt% Cu with a Cu surface area of 0.76 m^2 per gram of catalyst (2.1% Cu dispersion) and 30.5 wt% ZrO_2.

0021-9517/97 $25.00

Matheson UHP H_2 and He and Coleman instrument-purity CO_2 were purified prior to use. Hydrogen was passed through a Deoxo unit (Engelhard) to remove O_2 impurities by forming water which was subsequently removed by a molecular sieve trap (3A Davidson grade 564). He was passed through an oxysorb (CrO_2) trap to remove O_2 and then a molecular sieve trap. CO_2 was passed through a hopcalite trap (80% MnO_2 + 20% CuO) to remove CO and a molecular sieve trap to remove water. Purified gases were delivered to the infrared cell via Tylan Model FC-280 mass flow controllers.

In-situ transmission infrared spectroscopy was performed using 2-cm diameter catalyst disks of 0.2-mm thickness, weighing approximately 75 mg. The catalyst disks were contained in a low dead-volume infrared cell (20). Infrared spectra were collected using a Nicolet Magna 750 series II FTIR spectrometer. Signals were obtained from a narrow band MCT detector. *In situ* absorbance spectra were obtained by collecting 64 scans at 4 cm^{-1} resolution. Each spectrum was then referenced to a spectrum of the catalyst collected at the same temperature under He or H_2 flow, as appropriate. The cell is heated by electrical resistance heaters and the cell temperature was controlled by an Omega Series CN-2010 programmable temperature controller.

The methanol synthesis activity and selectivity were determined by placing 150 mg of catalyst into a micro-reactor connected to a gas manifold and operated at 0.65 MPa with a feed stream containing a 3/1 mixture of H_2 and CO_2. Product analysis was by mass spectrometry. A more complete description of the apparatus is given in Ref. (16).

Prior to each experiment with a fresh sample, the catalyst was reduced in 10% H_2/He flowing at 60 cm^3/min. The reduction temperature was raised at 2 K/min from ambient to 523 K, after which the catalyst was further reduced at 523 K for >8 h in pure H_2 flowing at 40 cc/min. Subsequent reductions were all performed at 523 K, but varied in time (always >8 h) to ensure that observable surface species were removed.

RESULTS

The activity and selectivity of Cu/SiO_2 and $Cu/ZrO_2/SiO_2$ are reported in Table 1. Under the conditions shown in Table 1, it is evident that zirconia addition increases the methanol synthesis activity of the catalyst by 13.1-fold, when activity is expressed on a per gram basis, and 27-fold when activity is expressed as a turnover frequency based on the number of Cu sites measured by N_2O titration. The effect of zirconia addition on the reverse-water–gas-shift (RWGS) reaction is much less pronounced, with a 2.2-fold increase in activity over Cu/SiO_2, when compared on a per-gram basis, and a 4.6-fold increase, when compared on a per-site basis. It is also evident that zirconia addition increases the selectivity to methanol 11 to 43%, while the RWGS selectivity is decreased from 88 to 56%. Internal and external heat and mass transfer effects on the rates of methanol synthesis and the RWGS reaction were determined to be negligible (21).

TABLE 1

Comparison of Methanol Synthesis and RWGS Activity and Selectivity[a]

	Catalyst[b]			
	Cu/SiO_2		$Cu/ZrO_2/SiO_2$	
	MeOH synthesis	RWGS reaction	MeOH synthesis	RWGS reaction
Mass specific rate (moles/s/g-cat)	9.9×10^{-8}	7.6×10^{-7}	1.3×10^{-6}	1.7×10^{-6}
Turnover frequency (1/s)	2.7×10^{-3}	2.0×10^{-2}	7.3×10^{-2}	9.3×10^{-2}
Selectivity (%)[c]	11	88	43	56

[a] Reaction conditions: $T = 523$ K, $P = 0.65$ MPa, $H_2/CO_2 = 3/1$, catalyst mass = 0.15 g.
[b] Catalyst composition described in experimental section.
[c] Balance due to methane formation.

Cu/SiO_2

CO_2 Adsorption

Figure 1 shows spectra obtained after CO_2 adsorption on Cu/SiO_2 at temperatures between 323 and 523 K. The catalyst was exposed to He/CO_2 at a ratio of 3/1 and a total pressure of 0.65 MPa for 90 min at each temperature. At 323 K features are observed at 1620 cm^{-1} for H_2O on SiO_2 (H_2O–Si), at 1602 cm^{-1} for H_2O on Cu (H_2O–Cu), at 1450 cm^{-1} for ionic (symmetrical) carbonate on Cu (i-CO_3–Cu), and at 1405 cm^{-1} for polydentate carbonate on Cu (p-CO_3–Cu) (22). Also observable are a peak at 1461 cm^{-1} for monodentate carbonate on Cu (m-CO_3–Cu) (23, 24), peaks at 1350, 1543, 2850, and 2928 cm^{-1} for bidentate formate on Cu (b-HCOO–Cu) (25), and a shoulder at 1361 cm^{-1} for monodentate formate on Cu (m-HCOO–Cu) (25). When CO_2 adsorption occurs at 373 K the peaks for p-CO_3–Cu (1405 cm^{-1}) and m-CO_3–Cu (1461 cm^{-1}) disappear, and the peaks for b-HCOO–Cu reach a maximum. At higher temperature, the peaks for b-HCOO–Cu decrease monotonically. Increasing temperature has little effect on the intensity of the peak for i-CO_3–Cu, but it does decrease the intensity of the peaks for H_2O on both Cu and SiO_2. Very weak features (not shown) are also observed at 2094 and 2077 cm^{-1} for CO adsorbed on Cu(110) and (111) surfaces, and at 2128 cm^{-1} for CO adsorbed on Cu^+ (26, 27). With increasing adsorption temperature these features become progressively smaller. The presence of b-HCOO–Cu may be the result of CO_2 reacting with hydrogen remaining on the Cu after reduction, even though the catalyst was

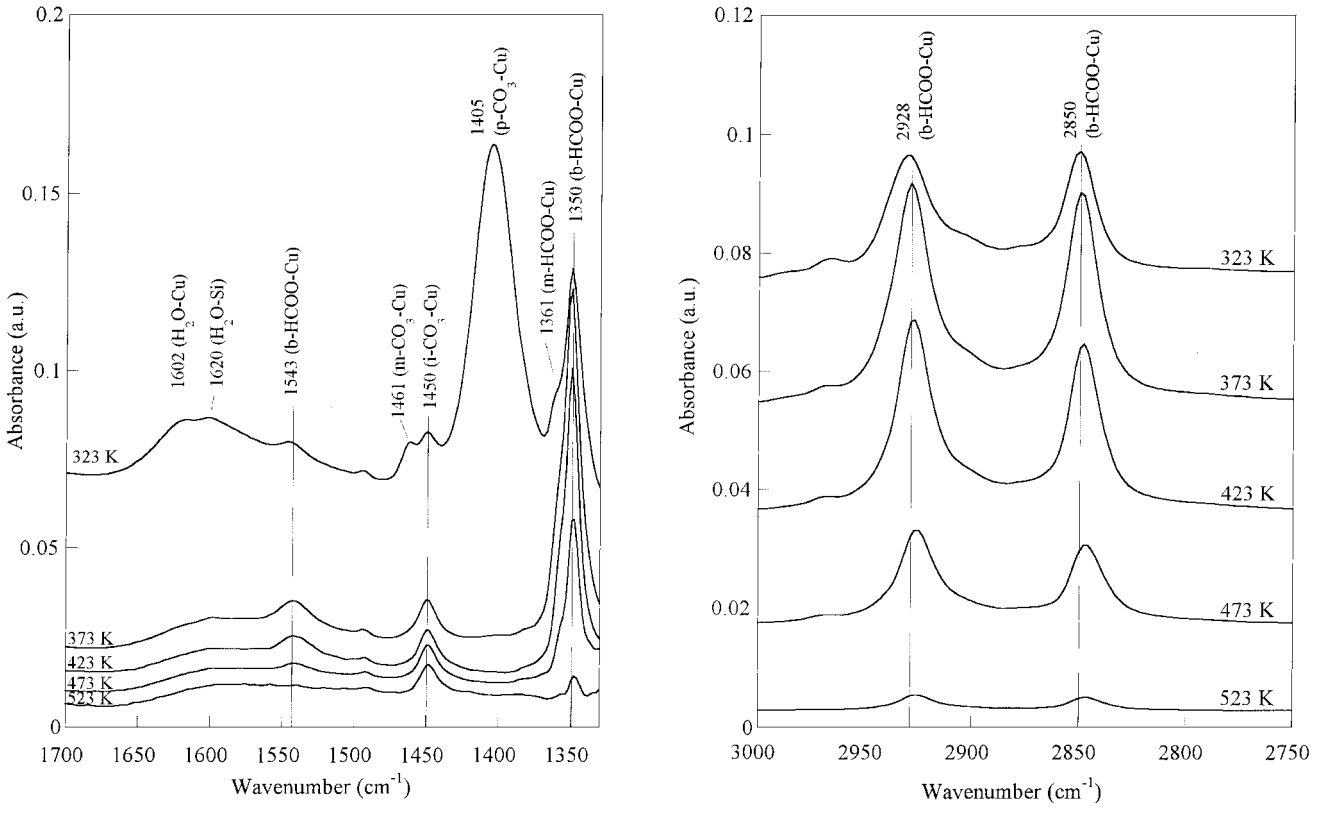

FIG. 1. Infrared spectra taken during exposure of Cu/SiO_2 to 0.16 MPa CO_2 and 0.49 MPa He flowing at a total rate of 60 cm^3/min. Spectra referenced to Cu/SiO_2 under 0.65 MPa He flow at each temperature.

purged at 523 K for 30 min in He to remove adsorbed hydrogen prior to cooling the catalyst to 323 K.

CO_2 Hydrogenation

Figure 2 shows spectra obtained at temperatures between 323 and 523 K while flowing H_2/CO_2 (3/1) over Cu/SiO_2 at a total pressure of 0.65 MPa. Spectra were collected after 5 h at each temperature. At 323 K, m-HCOO–Cu (1362(sh) cm^{-1}) is apparent but not at higher temperatures. The presence of b-HCOO–Cu (2931, 2853,1545, and 1352 cm^{-1}) is also observed at 323 K. With increasing temperature, the features associated with this species reach a maximum intensity at 373 K. At higher temperatures these features decay, but b-HCOO–Cu is still present at 523 K. A peak for i-CO_3–Cu (1450 cm^{-1}) is observable at all temperatures. Adsorbed H_2O on Cu (1601 cm^{-1}) is most apparent at 323 K. Weak features for adsorbed CO on Cu are present at all temperatures (not shown). CO on Cu(111) (2077 cm^{-1}) decreases with increasing temperature; CO on Cu(110) (2094 cm^{-1}) remains essentially constant with increasing temperature; and CO on Cu^+ (2128 cm^{-1}) increases with increasing temperature. At 373 to 473 K features at 1736, 1731, and 1658 cm^{-1} are observable, which are best ascribed to adsorbed formaldehyde on SiO_2 (CH_2O–Si, 1736 cm^{-1}) (28), methyl formate on SiO_2 (CH_3OCHO–Si, 1731 cm^{-1}) (28, 29), and methyl formate on Cu (CH_3OCHO–Cu, 1658 cm^{-1}) (28, 29). The features at 1371(sh) and 1467 cm^{-1} observable at 323–473 K are due to monodentate carbonate on Cu (m-CO_3–Cu) (23, 24). At 423–523 K features for methoxide on silica (CH_3O–Si) are also observable (2956 and 1462 cm^{-1}) (29–33).

Temporal Resolution of Surface Species

Transient spectra were obtained after switching the feed from H_2 to 3/1 H_2/CO_2 at a total pressure of 0.65 MPa while maintaining the temperature of the Cu/SiO_2 catalyst at 523 K. The results are shown in Fig. 3. b-HCOO–Cu (2927, 2849, 1540, 1350 cm^{-1}), and weak features for adsorbed CO on Cu (2128, 2094, 2077 cm^{-1}, not shown) form immediately upon switching and the intensities of the bands for these species remain relatively constant during the 22.6 h transient. At 2.7 min into the transient, a peak at 2959 cm^{-1} begins to grow in and increases in intensity during the remainder of the transient. This feature is ascribable to CH_3O–Si and the companion peak at 2856 cm^{-1} is evidenced by the asymmetry of the peak at 2849 cm^{-1} (shoulder on the left). CH_3O–Si is also evidenced by the shoulder at 2994 cm^{-1} and the bending mode observable at 1464 cm^{-1} at longer times. These features for CH_3O–Si have been observed during methanol adsorption on Cu/SiO_2 (30–33).

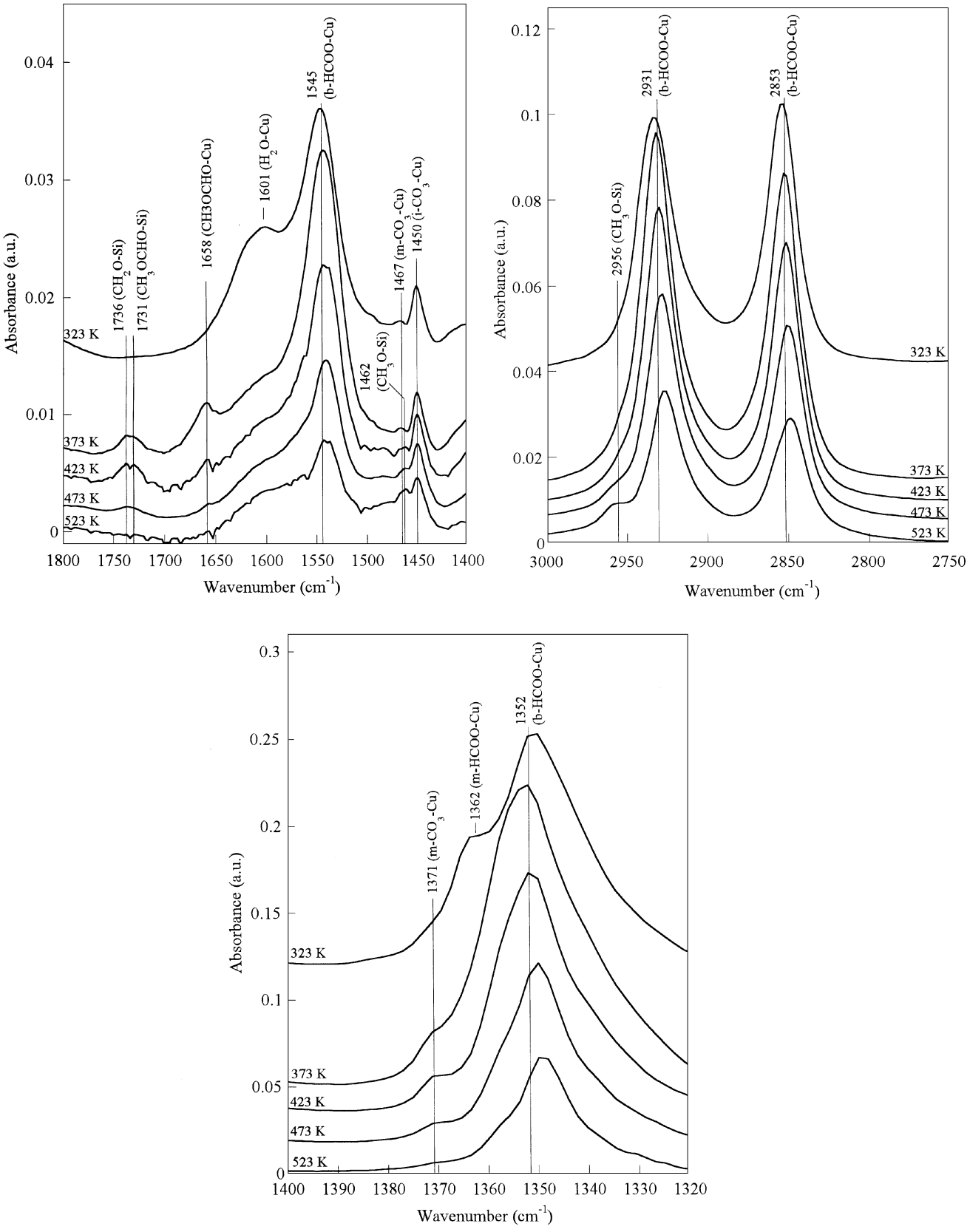

FIG. 2. Infrared spectra taken during exposure of Cu/SiO_2 to 0.16 MPa CO_2 and 0.49 MPa H_2 flowing at a total rate of 60 cm^3/min. Spectra referenced to Cu/SiO_2 under 0.65 MPa H_2 flow at each temperature.

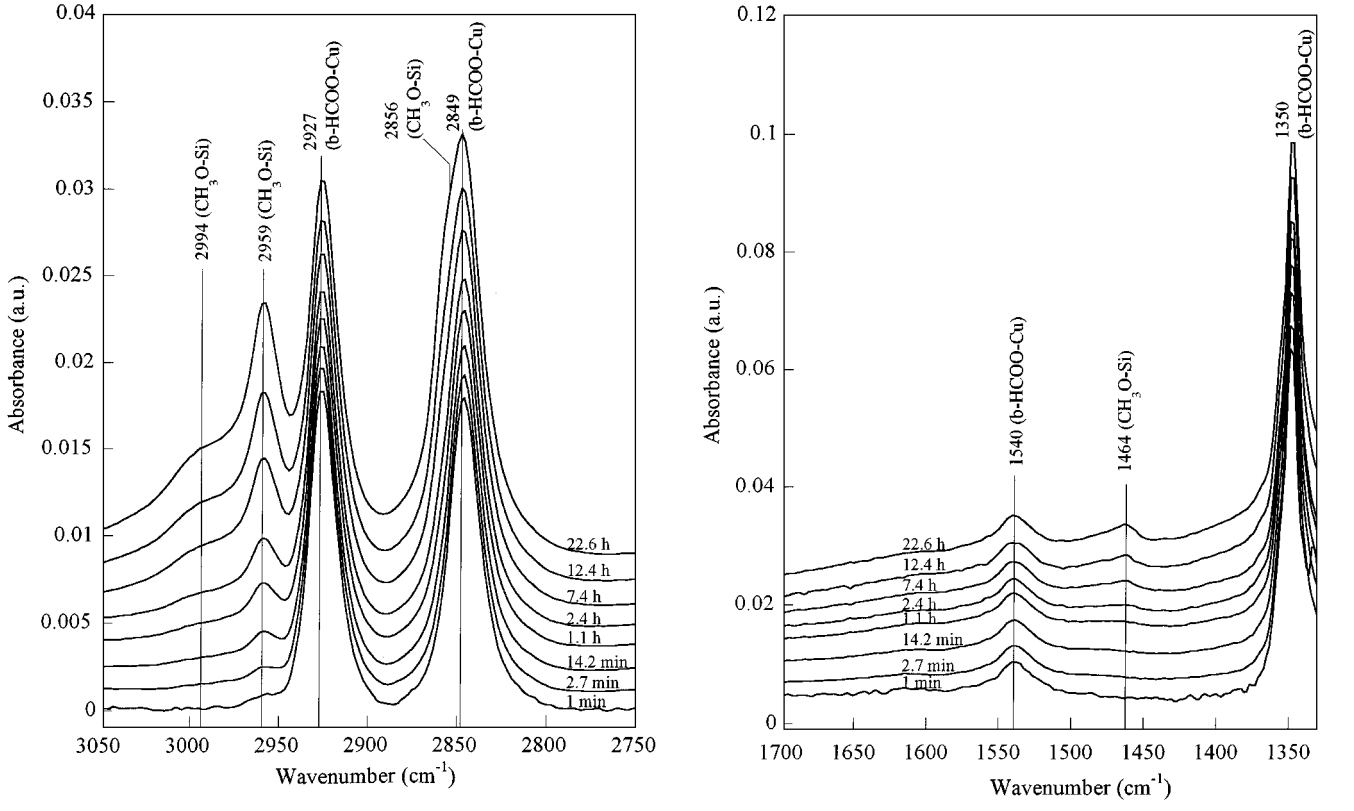

FIG. 3. Infrared spectra taken for Cu/SiO_2 at 523 K after switching the feed from 0.65 MPa H_2 to 0.16 MPa CO_2 and 0.49 MPa H_2 at a total rate of 60 cm^3/min. Spectra referenced to Cu/SiO_2 under 0.65 MPa H_2 flow at 523 K.

Transient spectra were obtained after switching the feed from 3/1 H_2/CO_2 to H_2 at a total pressure of 0.65 MPa while maintaining the temperature of the Cu/SiO_2 catalysts at 523 K. The results are shown in Fig. 4. After 30 s, CO on Cu (2094, 2077 cm^{-1}) is removed, while the CO on Cu (2128 cm^{-1}) decays more slowly during the transient (not shown). b-HCOO–Cu (2927, 2849, 1540, 1349 cm^{-1}) is removed in about 1 h. The contribution of CH_3O–Si at 2857 cm^{-1} is clearly observable at 0.6 min during the reduction. This peak and the remaining features due to CH_3O–Si (2992, 2959, and 1464 cm^{-1}) are the most persistent features observed during the transient.

ZrO_2/SiO_2 and $Cu/ZrO_2/SiO_2$

CO_2 Adsorption

Figure 5 shows spectra taken after ZrO_2/SiO_2 was exposed to He/CO_2 at a ratio of 3/1 and a total pressure of 0.65 MPa for 90 min at temperatures between 323 and 523 K. At 323 K the predominant features are bands at 1622 and 1435 cm^{-1}, which can be attributed to bidentate bicarbonate on ZrO_2 (b-HCO_3–Zr) (34–42) and ionic carbonate on ZrO_2 (i-CO_3–Zr) (34–37, 42), respectively. The peak for b-HCO_3–Zr which should be present at around 1465 cm^{-1} (wk) is most likely obscured by the high intensity feature at 1435 cm^{-1}. The feature at 1385 cm^{-1}, along with the very weak shoulder at 1480 cm^{-1}, is due to monodentate carbonate on zirconia (m-CO_3–Zr) (35–37, 40, 42, 43). The features at 1563 and 1356 cm^{-1} are due to bidentate carbonate on zirconia (b-CO_3–Zr) (34, 36, 37, 39–42). As the adsorption temperature is increased to 523 K, the band for b-HCO_3–Zr (1622 cm^{-1}) decreases significantly in intensity, and to a lesser extent so does the band for i-CO_3–Zr (1435 cm^{-1}). At 523 K the predominant species present are b-HCO_3–Zr (1622 cm^{-1}), b-CO_3–Zr (1563 cm^{-1}), and i-CO_3–Zr (1435 cm^{-1}). Weak bands at 2972 and 2894 cm^{-1} (not shown) and at 1386 and 1370 cm^{-1} suggest the formation of a small amount of bidentate formate on zirconia (b-HCOO–Zr) (19, 37–41, 43–45).

The formation of b-HCO_3–Zr is attributable to the reaction of CO_2 with hydroxyl groups present on the surface of the dispersed zirconia. Evidence for this interaction can be observed by examining the O–H stretching region of the spectrum. As shown in Fig. 5, bands with negative absorbances appear at 3775 and 3745 cm^{-1} when CO_2 is adsorbed on ZrO_2/SiO_2 at 323 K. The feature at 3775 cm^{-1} is associated with OH groups on monoclinic zirconia (40, 41, 46). Since the spectra in Fig. 5 are referenced to the reduced material, the presence of a negative band means that hydroxyl groups are consumed as a consequence of reaction

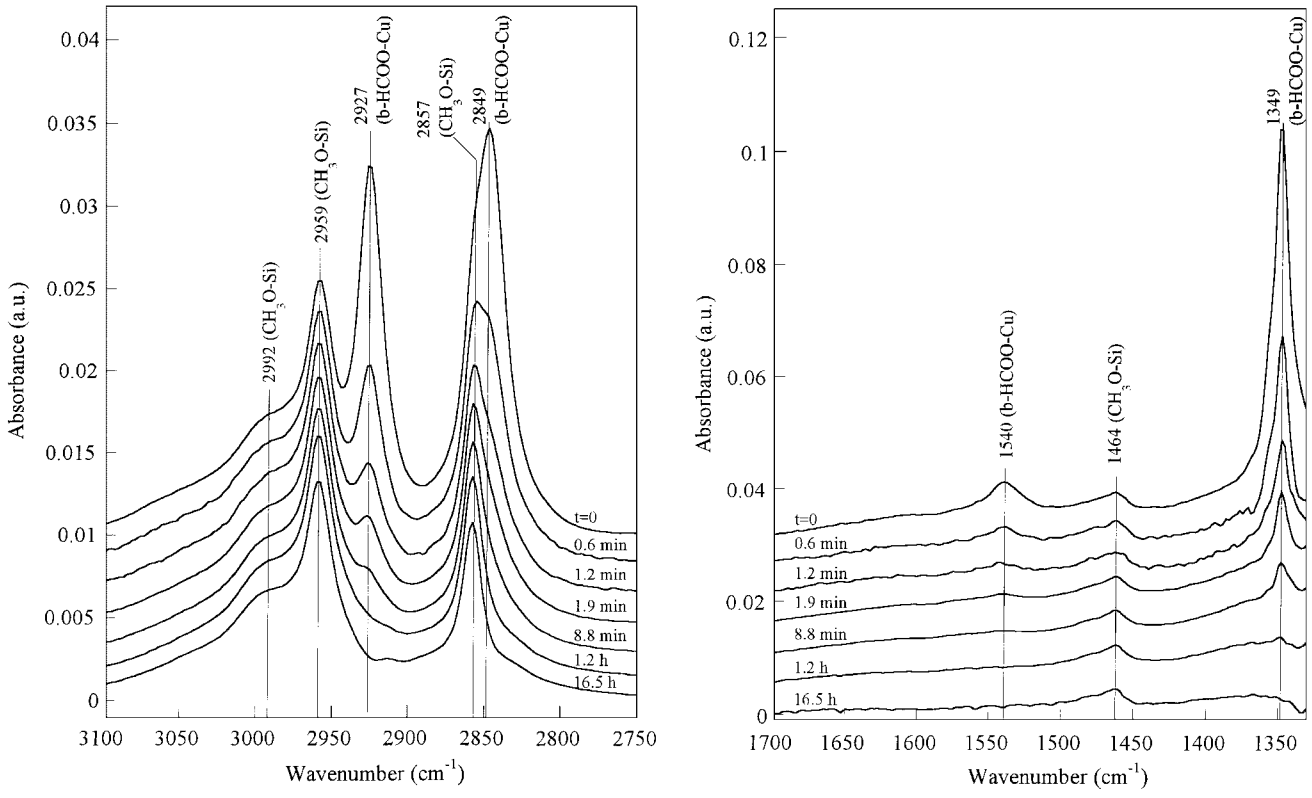

FIG. 4. Infrared spectra taken for Cu/SiO_2 at 523 K after switching the feed from 0.16 MPa CO_2 and 0.49 MPa H_2 to 0.65 MPa H_2 at a rate of 60 cm^3/min. Spectra referenced to Cu/SiO_2 under 0.65 MPa H_2 flow at 523 K.

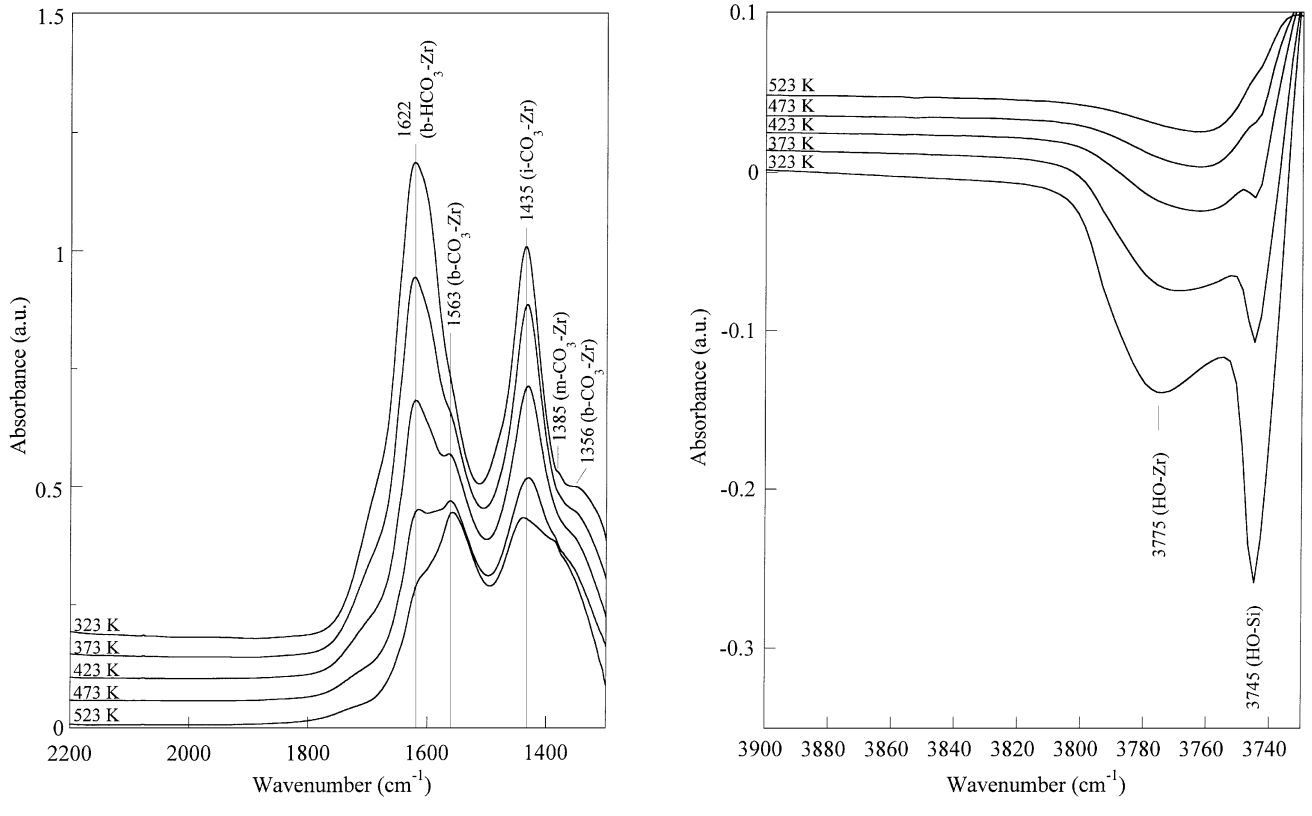

FIG. 5. Infrared spectra taken during exposure of ZrO_2/SiO_2 to 0.16 MPa CO_2 and 0.49 MPa He flowing at a total rate of 60 cm^3/min. Spectra referenced to ZrO_2/SiO_2 under 0.65 MPa He flow at each temperature.

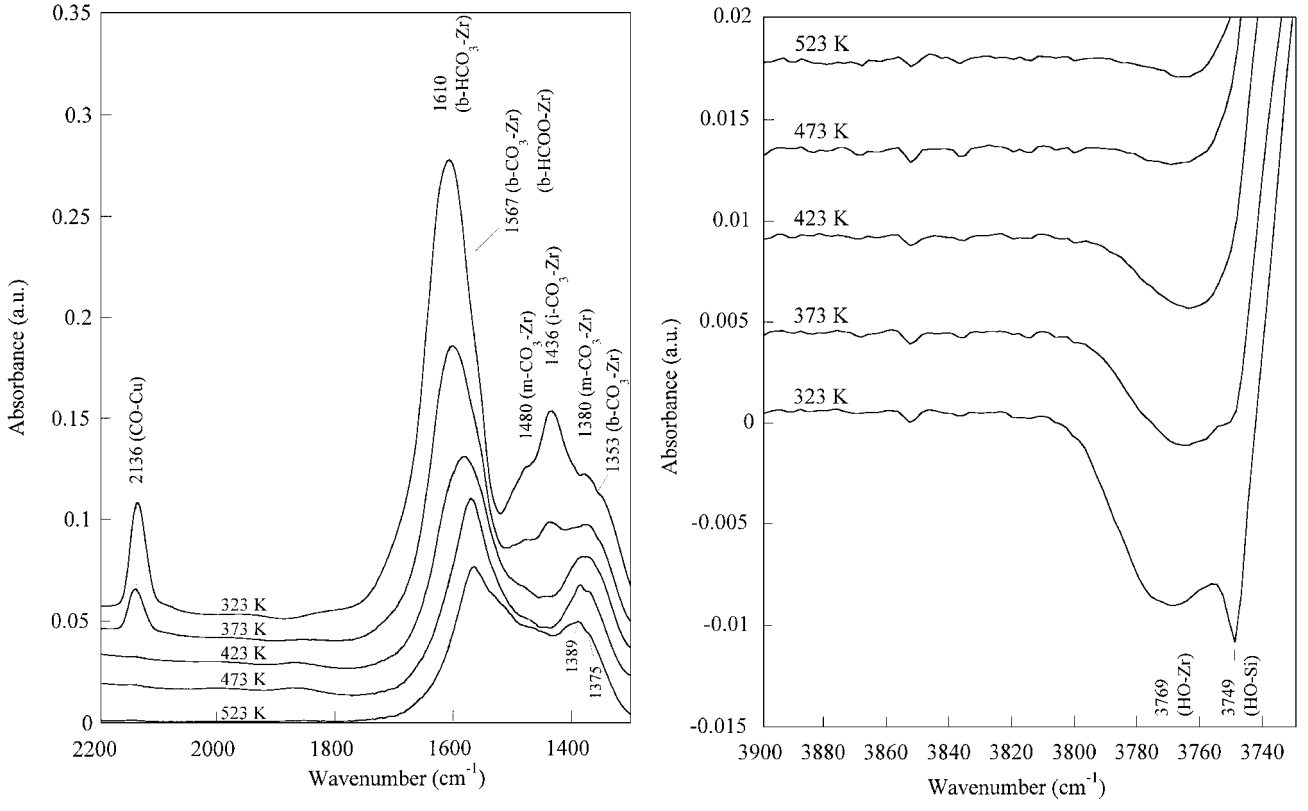

FIG. 6. Infrared spectra taken during exposure of $Cu/ZrO_2/SiO_2$ to 0.16 MPa CO_2 and 0.49 MPa He flowing at a total rate of 60 cm^3/min. Spectra referenced to $Cu/ZrO_2/SiO_2$ under 0.65 MPa He flow at each temperature.

with CO_2. The consumption of OH groups on zirconia coincides with the appearance of b-HCO_3–Zr (1622 cm^{-1}). When the adsorption temperature is raised to 523 K the hydroxyl band is largely recovered and the b-HCO_3–Zr band is diminished in intensity, indicating that b-HCO_3–Zr is less stable at this temperature. The band at 3745 cm^{-1} is attributed to isolated OH groups on SiO_2, as the behavior and position of this band is identical to that observed during CO_2 exposure to SiO_2 alone.

Figure 6 shows spectra obtained during the exposure of $Cu/ZrO_2/SiO_2$ to He/CO_2 at a ratio of 3/1 and a total pressure of 0.65 MPa for 90 min at temperatures between 323 and 523 K. The results are qualitatively similar to those for CO_2 adsorption on ZrO_2/SiO_2. At 323 K the principal features are those due to b-HCO_3–Zr (1610 cm^{-1}) and i-CO_3–Zr (1436 cm^{-1}). The features at 1380 and 1480 cm^{-1} are due to m-CO_3–Zr. The shoulder at 1353 cm^{-1} is due to b-CO_3–Zr, but the companion feature at about 1567 cm^{-1} is obscured by the intense b-CO_3–Zr peak at 1610 cm^{-1}. As the adsorption temperature is raised, the intensities of the bands for b-HCO_3–Zr, b-CO_3–Zr, i-CO_3–Zr, and m-CO_3–Zr decrease. At 523 K, the only distinguishable features remaining are the bands at 1567, 1389, and 1375 cm^{-1}. Weak bands are also observed at 2983 and 2900 cm^{-1} (not shown). All five of these features are attributable to b-HCOO–Zr. A portion of the intensity at 1567 cm^{-1} is attributed to b-CO_3–Zr. In contrast to what is observed for CO_2 adsorption on ZrO_2/SiO_2, a peak is seen at 2136 cm^{-1} due to CO on oxidized Cu (26, 27). This peak is not observed at temperatures above 373 K.

The formation of b-HCO_3–Zr is again attributable to the reaction of CO_2 with hydroxyl groups present on the surface of the dispersed zirconia. As shown in Fig. 6, a band with negative absorbance at 3769 cm^{-1}, attributable to OH groups on monoclinic zirconia, appears when CO_2 is adsorbed on $Cu/ZrO_2/SiO_2$ at 323 K. The consumption of OH groups on zirconia coincides with the appearance of b-HCO_3–Zr (1610 cm^{-1}). When the adsorption temperature is raised to 523 K the hydroxyl bands are recovered and the b-HCO_3–Zr band is not observed. The band at 3749 cm^{-1} is again due to OH groups on SiO_2.

CO_2 Hydrogenation

Figure 7 shows spectra obtained while flowing H_2/CO_2 at a ratio of 3/1 and a total pressure of 0.65 MPa at temperatures between 323 and 523 K on ZrO_2/SiO_2. Spectra were collected after 5 h at each temperature. The spectrum taken at 323 K is very similar to that observed for CO_2 adsorption (see Fig. 5). The principal features at 323 K are those for b-HCO_3–Zr (1619 cm^{-1}) and i-CO_3–Zr

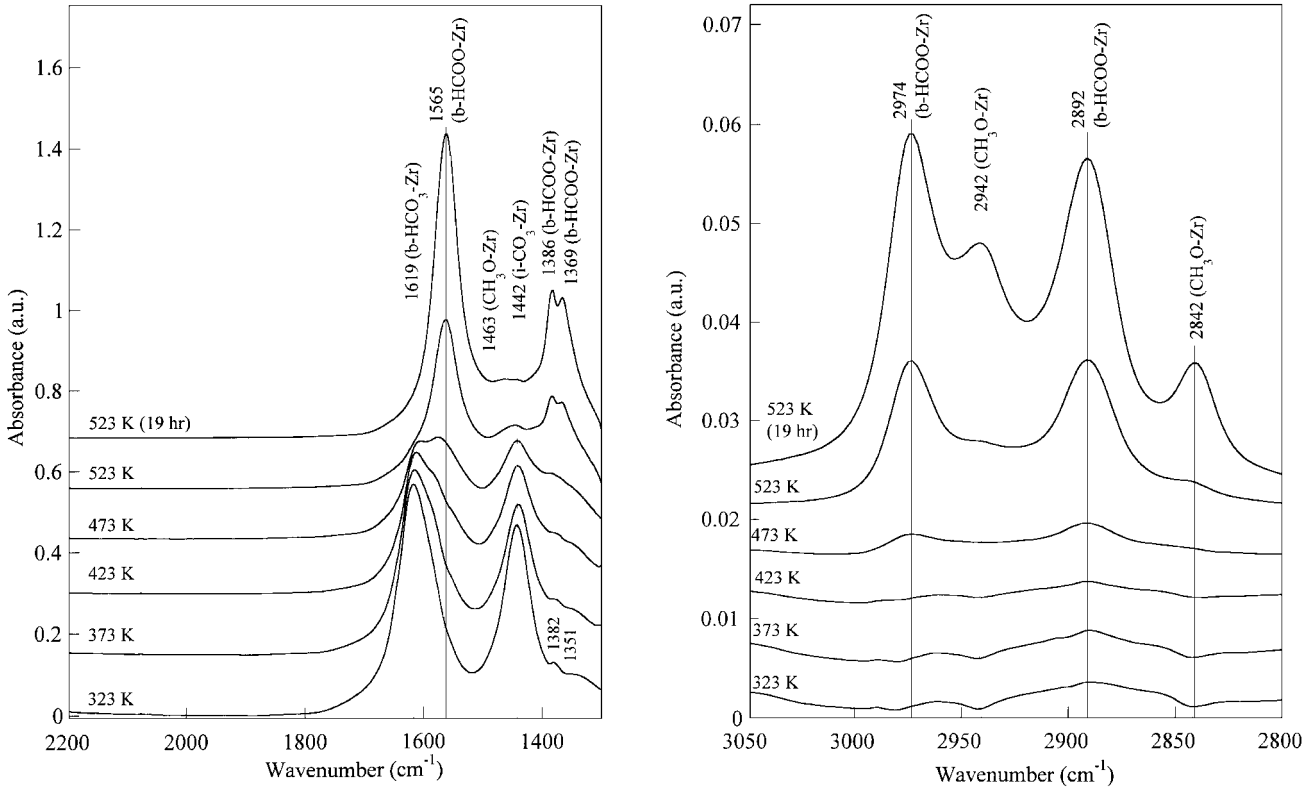

FIG. 7. Infrared spectra taken during exposure of ZrO_2/SiO_2 to 0.16 MPa CO_2 and 0.49 MPa H_2 flowing at a total rate of 60 cm^3/min. Spectra referenced to ZrO_2/SiO_2 under 0.65 MPa H_2 flow at each temperature.

(1442 cm^{-1}). A small amount of m-CO_3–Zr (1382 cm^{-1}) and b-CO_3–Zr (1351 cm^{-1}(sh)) are also present. As the temperature is increased, the concentrations of b-HCO_3–Zr and i-CO_3–Zr decrease and bands appear that are characteristic of b-HCOO–Zr (2974, 2892, 1565, 1386, 1369 cm^{-1}). At 523 K bands appear at 2942, 2842, and 1463 cm^{-1} which are attributable to methoxide species on zirconia (CH_3O–Zr) (19, 37–39, 41, 43, 45).

Figure 8 shows spectra obtained 5 h after exposure of $Cu/ZrO_2/SiO_2$ to flowing H_2/CO_2 (3/1) at a total pressure of 0.65 MPa and temperatures between 323 and 523 K. At 323 K the spectrum is comprised of features attributable to b-HCO_3–Zr (1606, 1465 cm^{-1}), m-CO_3–Zr (1490, 1383 cm^{-1}), b-CO_3–Zr (1576 cm^{-1}), and weak features for b-HCOO–Zr (2980, 2897, 1568, 1390, and 1370 cm^{-1}). In the temperature interval of 373–523 K b-HCOO–Zr (2980, 2897, 1568, 1389, and 1370 cm^{-1}) becomes the dominant species. With increasing temperature the intensities of the bands for this species pass through a maximum at 423 K. At 373 K new features appear at 2966 and 2861 cm^{-1} due to bidentate methylenebisoxy on zirconia (b-CH_2OO–Zr) (45, 47–50), and at 2944 and 2846 cm^{-1} due to CH_3O–Zr. At 473 K bands appear at 2957 and 2856 cm^{-1} due to CH_3O–Si. At 523 K, the features for b-CH_2OO–Zr are not readily apparent. In the C–O stretching region (not shown), peaks for CO on Cu (2131, 2094, 2077 cm^{-1}) are present at 323 K. The peak at 2131 cm^{-1} is gone at 373 K, while those at 2077 and 2094 cm^{-1} are present at all temperatures, but decrease in intensity with temperature.

Temporal Resolution of Surface Species

To investigate the dynamics of species interconversion, a series of experiments were conducted under both temperature-programmed and isothermal conditions. Figure 9 shows spectra taken after flowing 0.65 MPa CO_2 over $Cu/ZrO_2/SiO_2$ for 4 h at 323 K and after switching the flow to hydrogen at 0.65 MPa for 4 h at 323 K. Under CO_2 flow both bicarbonate and carbonates are observed. Upon switching the flow to hydrogen the intensities of features due to carbonates are greatly diminished, while those for bicarbonate retain much of their intensity. The temperature was then increased at 2 K/min under flowing hydrogen at 0.65 MPa, and the resulting spectra are shown in Fig. 10. From 396 to 523 K a systematic decrease can be seen in the intensity of the band (1607 cm^{-1}) for b-HCO_3–Zr and a corresponding rise in the intensity of the bands (1565, 1389, and 1370 cm^{-1}) for b-HCOO–Zr, providing clear evidence for the conversion of b-HCO_3–Zr to b-HCOO–Zr on $Cu/ZrO_2/SiO_2$.

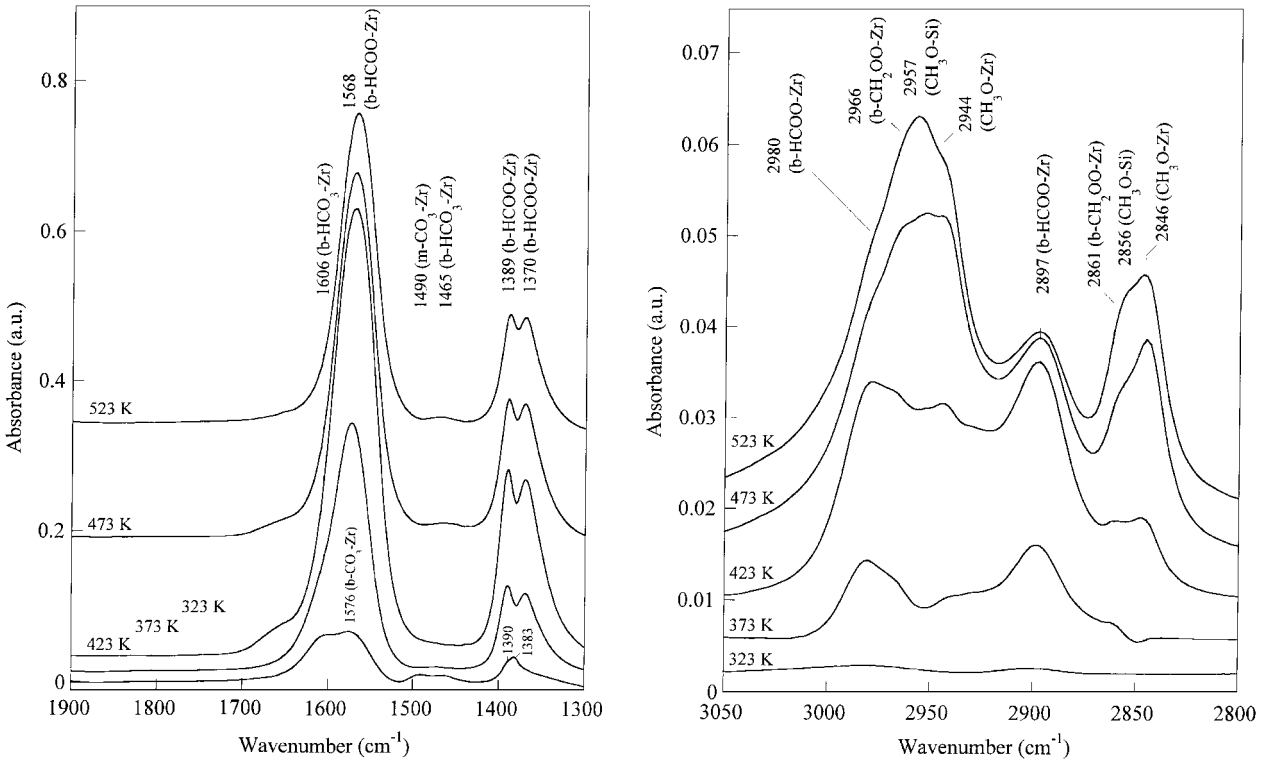

FIG. 8. Infrared spectra taken during exposure of $Cu/ZrO_2/SiO_2$ to 0.16 MPa CO_2 and 0.49 MPa H_2 flowing at a total rate of 60 cm^3/min. Spectra referenced to $Cu/ZrO_2/SiO_2$ under 0.65 MPa H_2 flow at each temperature.

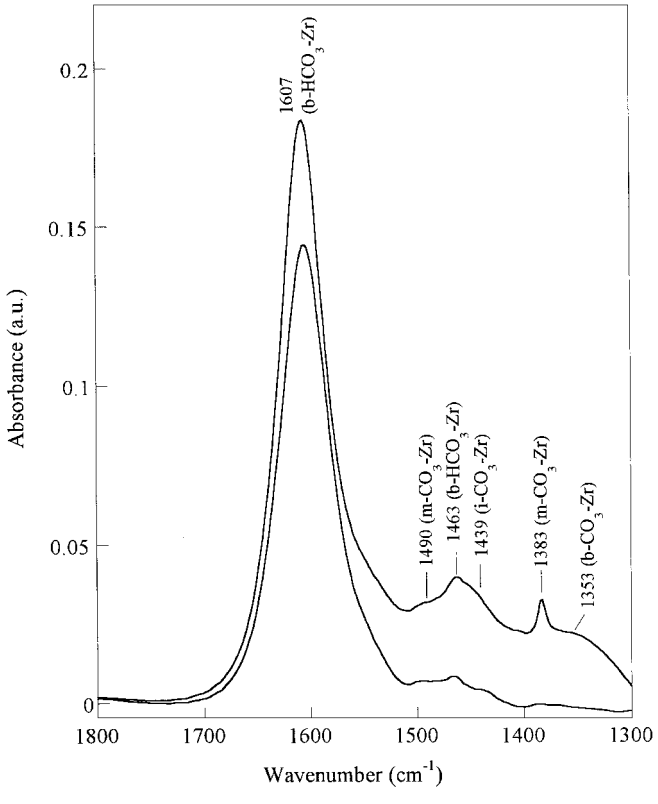

FIG. 9. Infrared spectra taken for $Cu/ZrO_2/SiO_2$ at 323 K. Top spectrum while flowing 0.65 MPa CO_2 at a rate of 60 cm^3/min for 4 h. Bottom spectrum while flowing 0.65 MPa H_2 at a rate of 60 cm^3/min for 4 h. Spectra referenced to $Cu/ZrO_2/SiO_2$ under 0.65 MPa H_2 flow at 323 K.

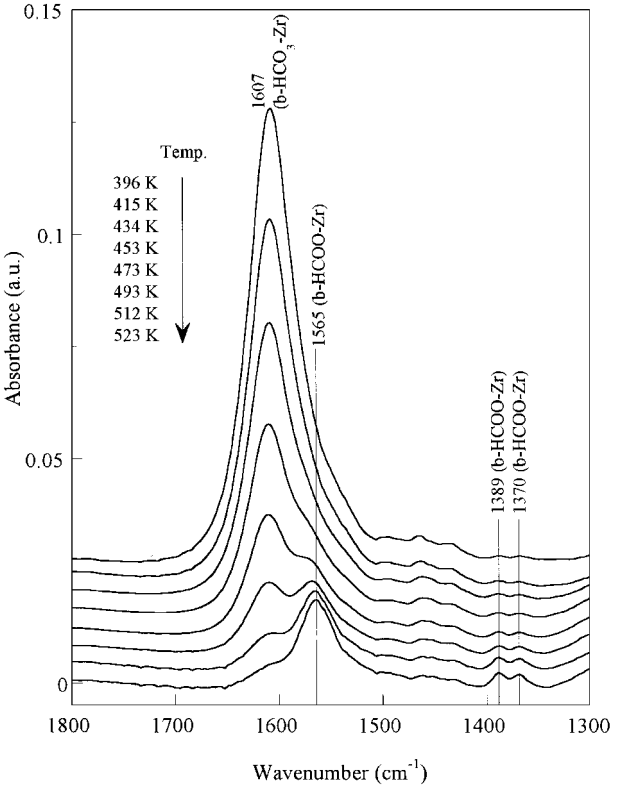

FIG. 10. Infrared spectra taken for $Cu/ZrO_2/SiO_2$ after exposure in Fig. 9 and increasing the temperature at 2 K/min under flowing 0.65 MPa H_2 at a rate of 60 cm^3/min. Spectra referenced to $Cu/ZrO_2/SiO_2$ under 0.65 MPa H_2 flow at each temperature.

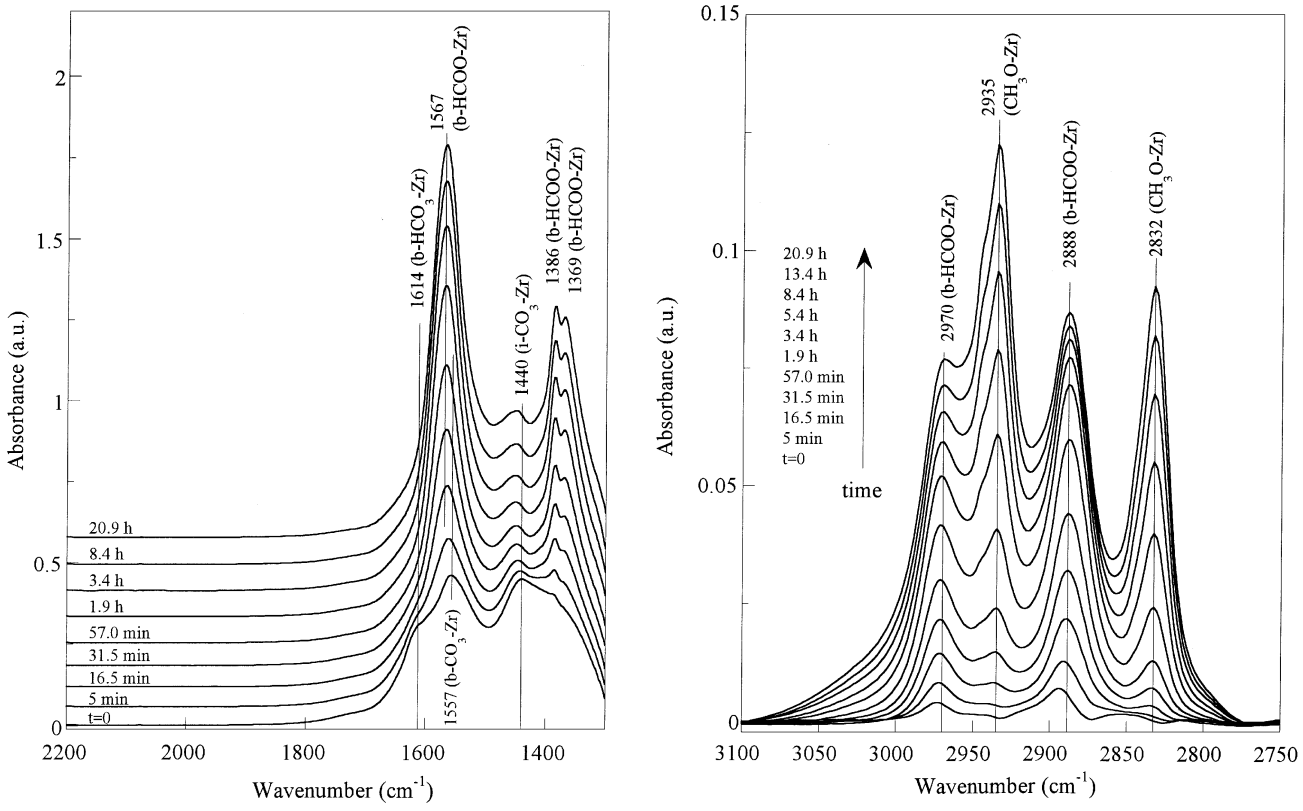

FIG. 11. Infrared spectra taken for ZrO_2/SiO_2 at 523 K after switching the feed from 0.49 MPa He and 0.16 MPa CO_2 to 0.49 MPa H_2 and 0.16 MPa CO_2 at a total rate of 60 cm^3/min. Flow switched after 2 h in He/CO_2. Spectra referenced to ZrO_2/SiO_2 under 0.65 MPa H_2 flow at 523 K.

Transient spectra were obtained after switching the feed from 3/1 He/CO_2 to 3/1 H_2/CO_2 at a total pressure of 0.65 MPa while maintaining the temperature of the ZrO_2/SiO_2 catalyst at 523 K. The results are shown in Fig. 11. At the beginning of the transient, b-HCO_3–Zr (1614 cm^{-1}), i-CO_3–Zr (1440 cm^{-1}), b-CO_3–Zr (1557 cm^{-1}), and b-HCOO–Zr (2970, 2888, 1567, 1386, and 1369 cm^{-1}) are present. As time progresses, the b-HCOO–Zr peaks in the region of 1300–1800 cm^{-1} increase in intensity and become dominant. After about 16.5 min, CH_3O–Zr (2935 and 2832 cm^{-1}) is observable, and the associated features grow in intensity during the remainder of the transient. After 21 h the intensity of the C–H bands for CH_3O–Zr become larger than those for b-HCOO–Zr. A weak band for i-CO_3–Zr (1450 cm^{-1} shifted from 1440 cm^{-1}) remains observable at long times.

Transient spectra were obtained after switching the feed from 3/1 He/CO_2 to 3/1 H_2/CO_2 at a total pressure of 0.65 MPa while maintaining the temperature of the Cu/ZrO_2/SiO_2 catalyst at 523 K. The results are shown in Fig. 12. At the beginning of the transient, b-HCO_3–Zr (1614 cm^{-1}) and b-HCOO–Zr (2982, 2899, 1564, 1389, 1371 cm^{-1}) are present. The formate features increase in intensity during the 16-h transient. Evidence for bicarbonate is gone after 3 min. After about 5.7 min, features for CH_3O–Zr (2949 and 2848 cm^{-1}) and CH_3O–Si (2955 cm^{-1}) become observable and increase in intensity during the remainder of the transient. After 24 min b-CH_2OO–Zr (2968 cm^{-1}) is present, and this feature increases in intensity at longer times. In the C–O stretching region (not shown), features due to CO on Cu (2130, 2094, and 2077 cm^{-1}) do not change in intensity upon switching from He/CO_2 to H_2/CO_2.

The dynamics of the appearance of b-HCOO–Zr and CH_3O–Zr on ZrO_2/SiO_2 and Cu/ZrO_2/SiO_2 during the experiments presented in Figs 11 and 12 are compared in Fig. 13. In each case, the peak intensity has been normalized to the value observed at the end of the transient. Also listed are the apparent first-order rate coefficients for the appearance of each species determined from the initial portion of the transient. It is evident that the formation of b-HCOO–Zr and CH_3O–Zr are significantly faster in the presence of Cu.

Transient spectra were obtained after switching the feed from 3/1 H_2/CO_2 to H_2 at a total pressure of 0.65 MPa while maintaining the temperature of the ZrO_2/SiO_2 catalyst at 523 K. The results are shown in Fig. 14. Features due to b-HCOO–Zr (2968, 2888, 1568, 1385, and 1370 cm^{-1}) decay very slowly over the 9.2-day transient. Features due to methoxide on ZrO_2 (2935 and 2833 cm^{-1}) increase in intensity during the first 5 days of the transient, then decay slowly, and persist even after 9 days. The feature for i-CO_3–Zr (1449 cm^{-1}) also decays only very slowly.

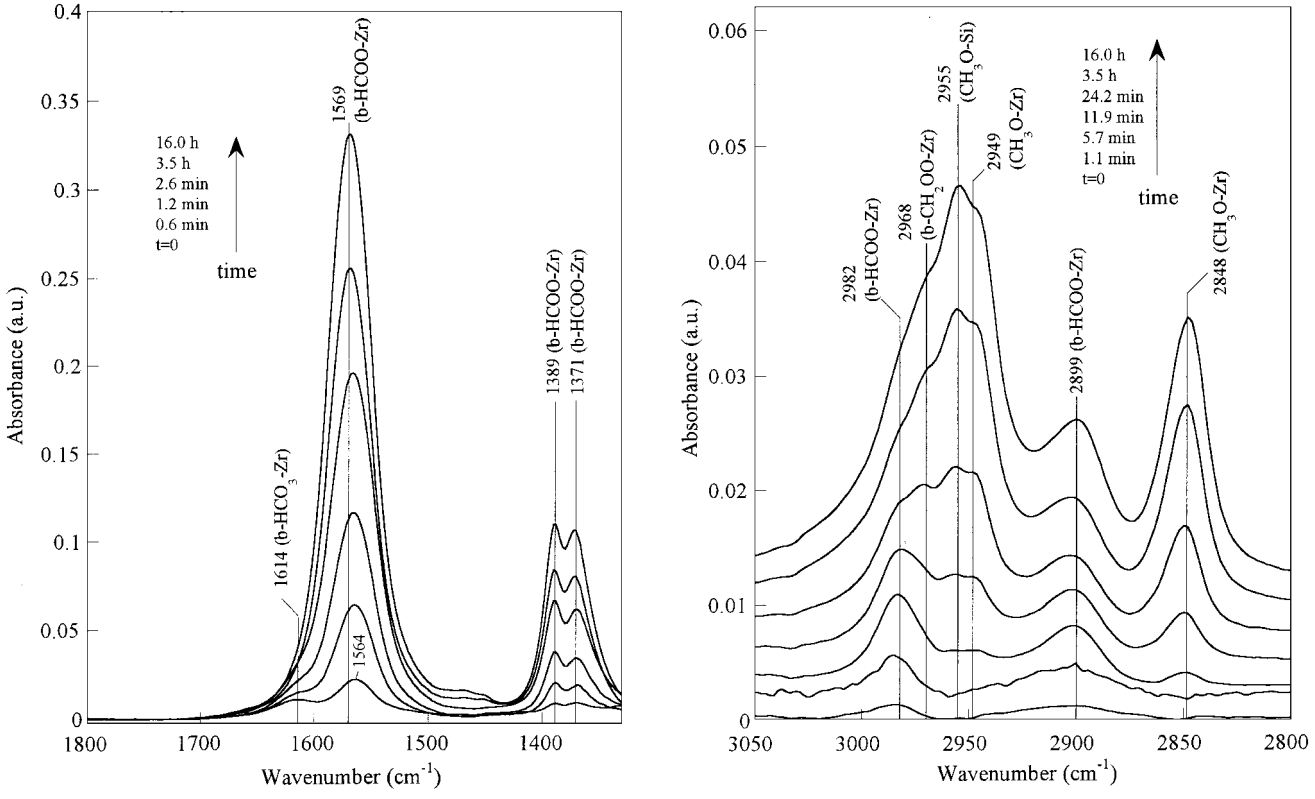

FIG. 12. Infrared spectra taken for $Cu/ZrO_2/SiO_2$ at 523 K after switching the feed from 0.49 MPa He and 0.16 MPa CO_2 to 0.49 MPa H_2 and 0.16 MPa CO_2 at a total rate of 60 cm^3/min. Flow switched after 2 h in He/CO_2. Spectra referenced to $Cu/ZrO_2/SiO_2$ under 0.65 MPa H_2 flow at 523 K.

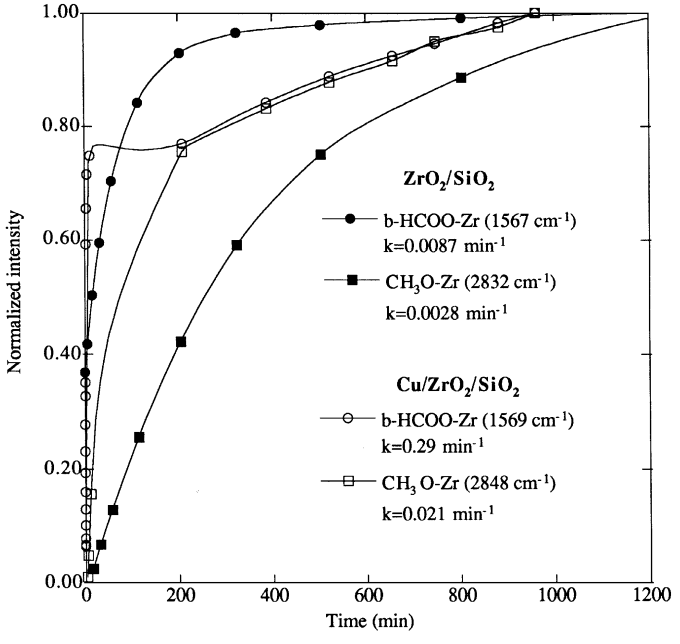

FIG. 13. Intensities of b-HCOO−Zr and CH_3O−Zr features for both ZrO_2/SiO_2 and $Cu/ZrO_2/SiO_2$ during the experiments in Figs. 11 and 12. Intensities normalized to those observed at the end of the transient.

Transient spectra were obtained after switching the feed from 3/1 H_2/CO_2 to H_2 at a total pressure of 0.65 MPa while maintaining the temperature of the $Cu/ZrO_2/SiO_2$ catalyst at 523 K. The results are shown in Fig. 15. In the C−H stretching region, b-HCOO−Zr (2978 and 2900 cm^{-1}) and b-CH_2OO−Zr (2967 cm^{-1}) decay most rapidly. Rapid loss of b-HCOO−Zr is also evident from inspection of the portion of the spectrum between 1300 and 1700 cm^{-1}. The features due to CH_3O−Si (2955 and 2855 cm^{-1}) and CH_3O−Zr (2945 and 2846 cm^{-1}) decay more slowly.

Figure 16 compares the dynamics for the consumption of b-HCOO−Zr and CH_3O−Zr on ZrO_2/SiO_2 and $Cu/ZrO_2/SiO_2$ when the feed is switched from H_2/CO_2 to H_2 at 523 K and a total pressure of 0.65 MPa (Figs. 14 and 15). Shown is the peak intensities for b-HCOO−Zr and CH_3O−Zr normalized to their maximum intensities observed at the beginning of the transient. Also shown is the apparent first-order rate constant for b-HCOO−Zr decay on both catalysts, and for the decay of CH_3O−Zr on $Cu/ZrO_2/SiO_2$. The result shows that formate and methoxide decay occurs much more readily on the copper containing catalyst and that methoxide decays only extremely slowly on ZrO_2/SiO_2.

The hydrolysis of CH_3O−Zr was investigated by reacting the residual methoxide remaining at the ends of the

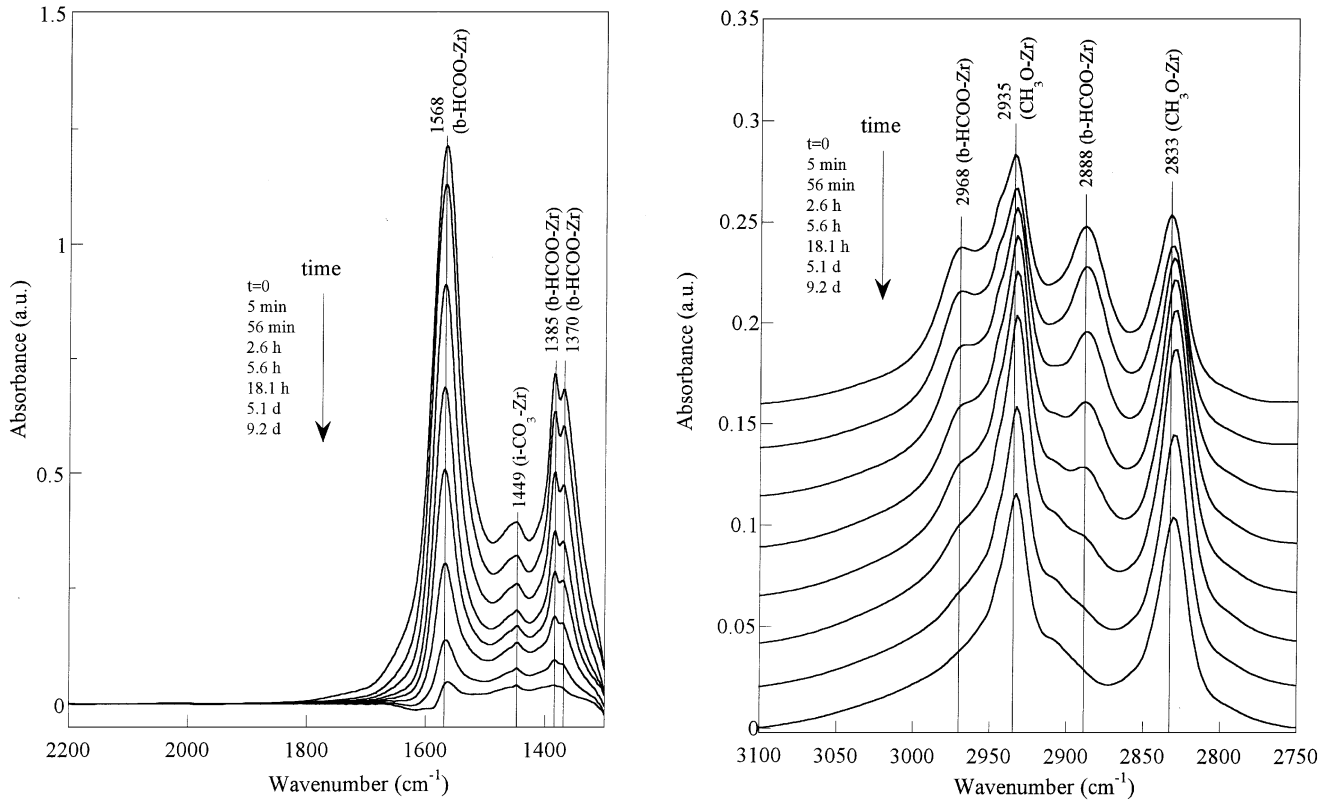

FIG. 14. Infrared spectra taken for ZrO_2/SiO_2 at 523 K after switching the feed from 0.49 MPa H_2 and 0.16 MPa CO_2 to 0.65 MPa H_2 at a rate of 60 cm^3/min. Flow switched after 21 h in H_2/CO_2. Spectra referenced to ZrO_2/SiO_2 under 0.65 MPa H_2 flow at 523 K.

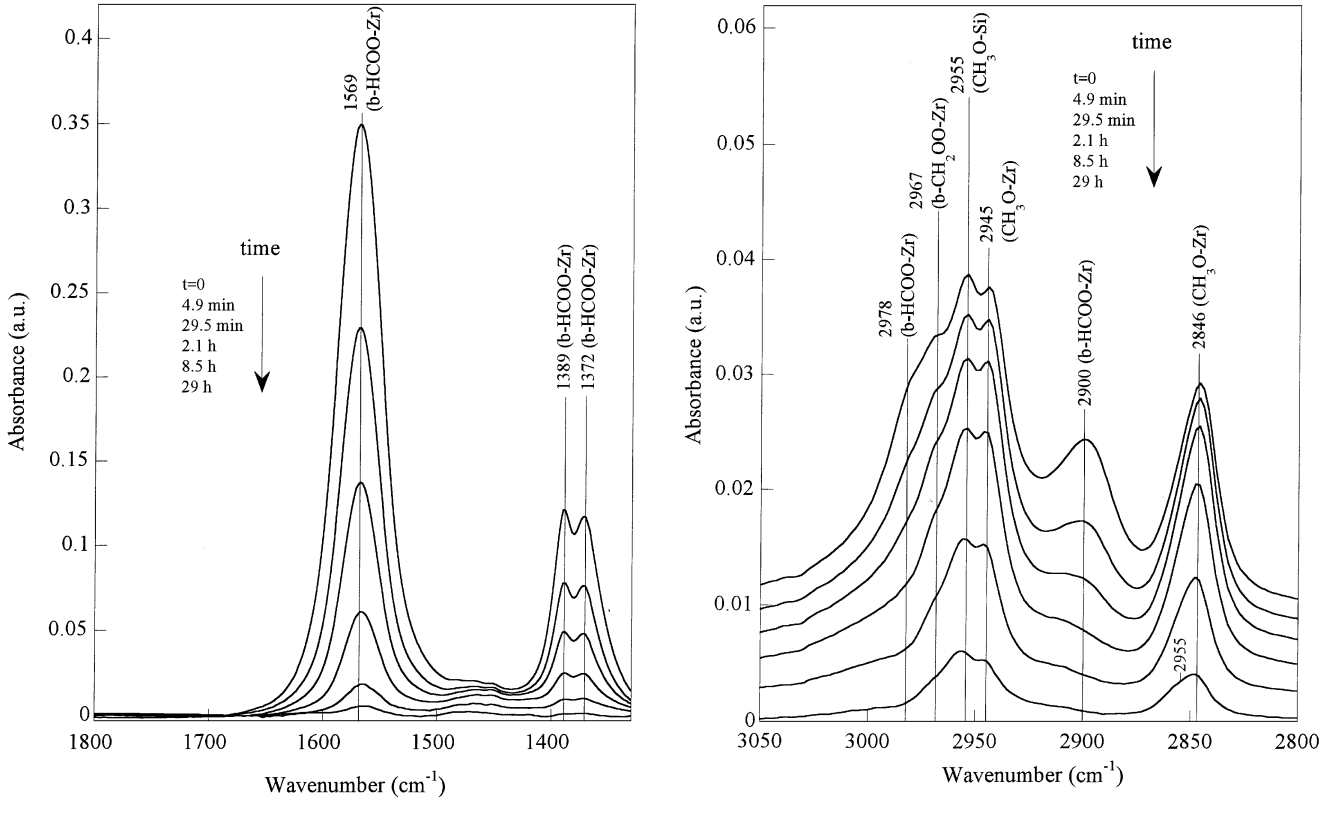

FIG. 15. Infrared spectra taken for $Cu/ZrO_2/SiO_2$ at 523 K after switching the feed from 0.49 MPa H_2 and 0.16 MPa CO_2 to 0.65 MPa H_2 at a rate of 60 cm^3/min. Flow switched after 20 h in H_2/CO_2. Spectra referenced to $Cu/ZrO_2/SiO_2$ under 0.65 MPa H_2 flow at 523 K.

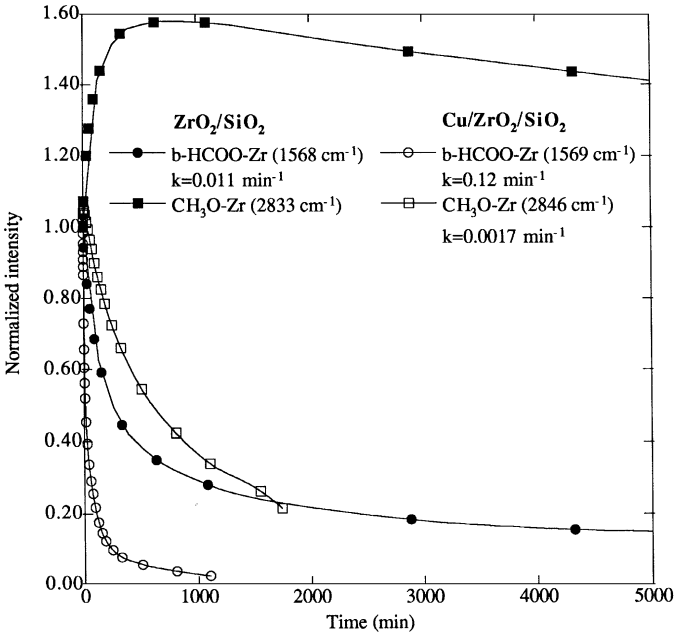

FIG. 16. Intensities of b-HCOO–Zr and CH_3O–Zr features for both ZrO_2/SiO_2 and $Cu/ZrO_2/SiO_2$ during the experiments in Figs. 14 and 15. Intensities normalized to those observed at the beginning of the transient.

transients in Figs. 14 and 15 with H_2 saturated with H_2O ($P_{H_2O} = 3.2$ kPa) at 523 K and 0.1 MPa total pressure. Only methoxide was present on the catalysts in significant quantities at the beginning of the transients. The results are shown in Fig. 17. Shown are the peak intensities for methoxide normalized to their intensities observed at the beginning of the transient. The results show that methoxide decays at a much faster rate in H_2/H_2O than in H_2 for both catalysts. It is also evident that the methoxide decay rate in H_2/H_2O is the same whether Cu is present or not.

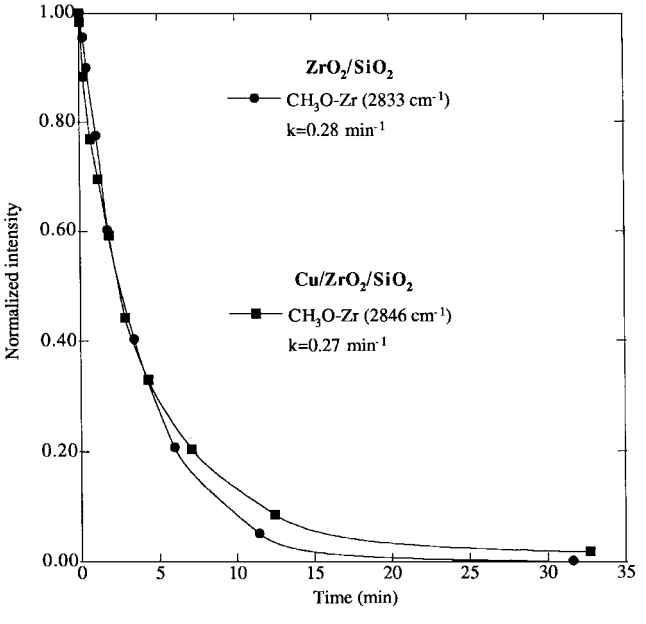

FIG. 17. Intensities of CH_3O–Zr features for both ZrO_2/SiO_2 and $Cu/ZrO_2/SiO_2$ after switching feed from 0.10 MPa H_2 to H_2O saturated ($P_{H_2O} = 3.2$ kPa) H_2 at a total pressure of 0.10 MPa and a total rate of 60 cm^3/min at 523 K. Intensities normalized to those observed at the beginning of the transient.

DISCUSSION

As noted in the Introduction, studies by a number of investigators have demonstrated that Cu supported on zirconia is exceptionally active for methanol synthesis from both CO_2 and CO. Likewise the results presented in Table 1 and those previously reported by the present authors show that the addition of zirconia to Cu/SiO_2 progressively enhances the activity of the catalyst for methanol synthesis from CO_2 by up to 35-fold at 473 K (16). Therefore, it is of interest to consider the ways in which the presence of zirconia either as a support or an additive enhances the rate of methanol synthesis. The first possibility is that zirconia acts independently of copper, since zirconia is known to be a catalyst for the synthesis of methanol (45, 51). This interpretation can be quickly ruled out since ZrO_2 exhibits no measurable activity for methanol synthesis from CO_2 under the conditions of the present study (16). The second possibility is that zirconia promotes the rate of methanol formation occurring on the surface of Cu, or alternatively that Cu promotes the synthesis of methanol over zirconia. Which of these latter two options offers the most plausible explanation requires a consideration of the observables.

Figure 2 shows that, in the absence of zirconia, the principal adsorbed species present on the surface of Cu/SiO_2 during methanol synthesis is b-HCOO–Cu. Above 423 K, CH_3O–Si species are observed as well, due to either the spillover of methoxide species from Cu or the re-adsorption of gas-phase methanol. Previous mechanistic studies conducted with Cu/SiO_2 suggest that the methanol is formed via the stepwise hydrogenation of b-HCOO–Cu to form methylenebisoxy and then methoxide species, the final precursor to methanol (see, for example, Ref. (52) and the references cited therein).

In the presence of zirconia, virtually all of the adsorbed species observed by infrared spectroscopy occur on the surface of zirconia irrespective of whether or not Cu is present. Although b-HCOO–Cu forms readily on Cu/SiO_2 during CO_2 hydrogenation, b-HCOO–Cu was not observed on $Cu/ZrO_2/SiO_2$. In the absence of hydrogen, CO_2 adsorption gives very similar results for both ZrO_2/SiO_2 and $Cu/ZrO_2/SiO_2$, forming bicarbonate and carbonates on zirconia (see Figs. 5 and 6). In the presence of both H_2 and CO_2, the influence of Cu is evidenced by b-HCOO–Zr formation at 373 K on $Cu/ZrO_2/SiO_2$, but only at 473 K on ZrO_2/SiO_2. Also, CH_3O–Zr formation is observed at 423 K on $Cu/ZrO_2/SiO_2$, but only at 523 K on ZrO_2/SiO_2 (see Figs. 7 and 8). The transient response data appearing in

Fig. 13 show very clearly that Cu enhances the rate of formation of b-HCOO–Zr and the rate at which this species is converted to CH_3O–Zr. The presence of Cu also enhances the rate of hydrogenation of b-HCOO–Zr and the rate of reductive elimination of CH_3O–Zr (see Fig. 16). Since atomic hydrogen is required for both processes and since Cu is more effective than ZrO_2 in dissociating H_2 (55), the observations noted above suggest that Cu is responsible for supplying atomic hydrogen required for the hydrogenation reactions occurring on ZrO_2. Previous work on a Cu/SiO_2 catalyst similar to that used in the present study has shown that H_2 adsorbs dissociatively on Cu with a heat of adsorption of about 12 kcal/mol and an activation barrier of about 10.5 kcal/mol (53). Thus, it seems reasonable to suggest that $Cu/ZrO_2/SiO_2$ acts as a bifunctional catalyst. The Cu serves to dissociatively adsorb H_2 and provide a source of atomic hydrogen by spillover, whereas the ZrO_2 serves to adsorb CO_2 as bicarbonate and carbonate species which then undergo stepwise hydrogenation to methanol. Additional methanol may be formed over Cu itself. This view of methanol synthesis over $Cu/ZrO_2/SiO_2$ has been recently suggested by the present authors (16) and a similar but less detailed picture has been proposed by Bianchi *et al.* (43). The processes envisioned to occur on ZrO_2 are similar to those proposed earlier to explain methanol synthesis on zirconia (45, 51), and attention has been drawn recently to the importance of hydrogen spillover during methanol synthesis on Cu/ZnO (54).

Based on the preceding arguments, a possible mechanism for CO_2 hydrogenation to methanol in the presence of Cu and zirconia is offered in Fig. 18. In this scheme, Cu and ZrO_2 are envisioned to be in close proximity. CO_2 adsorption leads to either carbonate or bicarbonate species on zirconia. In the absence of H_2, both species are observed at temperatures up to 423 K, but at 473 K and above, only the carbonate species are stable (see Fig. 6). In the presence of H_2, carbonate species are readily converted to bicarbonate species, and this process occurs already at 423 K (see Fig. 9). The involvement of Zr–OH groups in the formation of bicarbonate groups is evidenced by the consumption of Zr–OH groups upon adsorption of CO_2, and the concurrent appearance of the band at 1610–1622 cm^{-1} associated with $\nu(CO_2)_a$ vibrations of b-HCO_3 (see Figs. 5 and 6). The spectra in Fig. 10 show that above 453 K bicarbonate species are converted to formate. Since this later process is competitive with the decomposition of b-HCO_3–Zr to CO_2 and Zr–OH, high surface concentrations of b-HCOO–Zr are not observed unless gas phase CO_2 is present at elevated pressure. When both H_2 and CO_2 are present in the gas phase b-HCOO–Zr is observed already at 373 K (see Fig. 8).

Our previous studies have shown that under reaction conditions identical to those used here and with the same catalyst, the rate for methanol formation is insignificant below

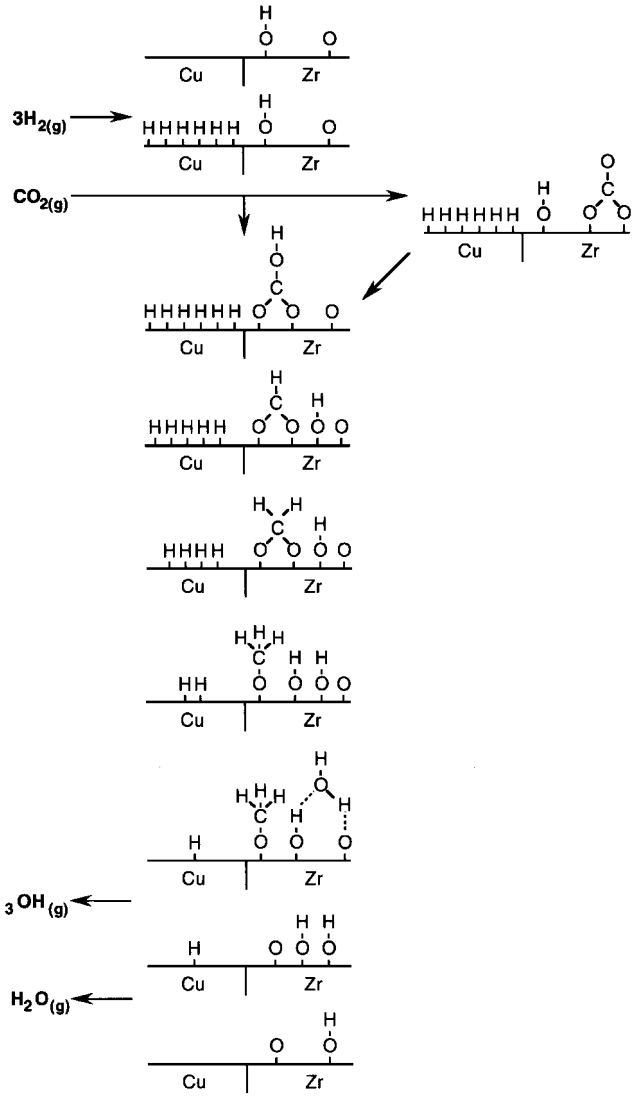

FIG. 18. Proposed mechanism for the synthesis of methanol from CO_2 and H_2 on Cu- and ZrO_2-containing catalysts.

423 K (16). Consistent with this, the *in-situ* infrared spectra presented in Fig. 8 show that methoxide species are not formed in significant concentration below this temperature. The concurrent appearance of bands for methylenebisoxy species strongly supports the proposal that these species are intermediates in the conversion of b-HCOO–Zr to CH_3O–Zr. While the reductive elimination of CH_3O–Zr does occur (see Fig. 16) this process is slow relative to the hydrolysis of CH_3O–Zr (see Fig. 17). Methoxide hydrolysis has been shown to be facile on Cu/ZnO (55), and is suggested to be more favorable than methoxide hydrogenation by thermodynamic calculations (3). Methoxide hydrolysis has also been shown to occur on zirconia at 398 K, while methanol synthesis from H_2/CO_2 occurs at 873 K (45). This again points to the role of Cu in supplying

hydrogen. CuO/ZrO_2 has been shown to produce water after hydrogen adsorption during temperature-programmed reduction, while ZrO_2 does not (56). In the presence of Cu, water readily forms and hydrolysis of methoxide to methanol results. In the absence of Cu, water does not form as readily and hydrogenation of methoxide to methanol is dominant. When water is introduced in the feed, methoxide hydrolysis occurs at the same rate, whether or not Cu is present (see Fig. 17), as would be expected, based on the above discussion.

The ratio of the rate of methoxide hydrolysis to the rate of methoxide hydrogenation can be estimated from the measured apparent first-order rate coefficients. During steady state reaction of 0.49 MPa H_2 and 0.16 MPa CO_2 on $Cu/ZrO_2/SiO_2$ at 523 K, the total conversion of CO_2 was measured to be 4.2% (16), corresponding to a water partial pressure of 6.8 kPa. The methoxide hydrolysis experiments shown in Fig. 17, were conducted at a water partial pressure of 3.2 kPa. Correcting the apparent rate constant for methoxide hydrolysis (Fig. 17) to a water partial pressure of 6.8 kPa yields a value of 0.57 min^{-1}. The apparent rate constant for methoxide hydrogenation on $Cu/ZrO_2/SiO_2$ is 0.0017 min^{-1} (Fig. 16). It is clear, therefore, that the rate of methoxide hydrolysis is about 340 times faster than the rate of reductive elimination. This suggests that water formed as a co-product of methanol synthesis from CO_2, as well as the RWGS reaction, is instrumental in the formation of methanol from methoxide species on $Cu/ZrO_2/SiO_2$.

Figures 13 and 16 clearly demonstrate that the presence of Cu greatly increases the rates at which b-HCOO–Zr and CH_3O–Zr form and are consumed. It is also important to observe that both in the absence and presence of Cu the surface concentration of CH_3O–Zr passes through a maximum, while the surface concentration of b-HCOO–Zr decreases monotonically, when the feed to the catalyst is switched from H_2/CO_2 to H_2 (see Fig. 16). However, the methoxide maximum occurs much sooner in the presence of Cu. If methoxide removal with hydrogen were fast, compared to its formation from formate, this maximum would not be observed. Based on the dynamics with which various species are formed and consumed, it is possible to deduce that on $Cu/ZrO_2/SiO_2$, the rate of formation of b-HCOO–Zr from CO_2 is roughly 2.5 times faster than the rate at which b-HCOO–Zr undergoes hydrogenation to CH_3O–Zr.

As demonstrated in Table 1, the addition of ZrO_2 to Cu/SiO_2 has relatively little influence on the rate of the reverse-water–gas-shift (RWGS) reaction. This suggests that the RWGS reaction occurs principally on Cu. Consistent with this interpretation, Bianchi *et al.* (44) report that CO derived from the decomposition of formate species adsorbed on ZrO_2 occurs in the vicinity of 623 K, a temperature considerably higher than that at which methanol synthesis from CO_2 occurs. The mechanism via which the RWGS occurs has been the subject of debate. While some authors conclude that CO is formed as a consequence of the dissociative adsorption of CO_2 on Cu (57–60), others have presented data supporting CO formation due to the decomposition of b-HCOO–Cu species (23, 61–63).

CONCLUSIONS

The locus of methanol synthesis from CO_2/H_2 over Cu/SiO_2 and $Cu/ZrO_2/SiO_2$ are found to be quite different. In the former case, the hydrogenation of CO_2 to methanol occurs on Cu. CO_2 adsorbs on Cu to form carbonate species, but in the presence of H_2 these species are rapidly converted to formate species adsorbed on Cu. The later species undergo stepwise hydrogenation to methanol. For $Cu/ZrO_2/SiO_2$, virtually all of the adsorbed species are associated with ZrO_2. CO_2 adsorbs as carbonate and bicarbonate species, which then react with atomic hydrogen to form formate species, and eventually, methoxide species, all of which are adsorbed on ZrO_2. The presence of Cu greatly accelerates these transformations, as well as the reductive elimination of methoxide species as methanol. However, the release of methanol via the hydrolysis of methoxide species on ZrO_2 is found to be significantly more rapid than reductive elimination. A bifunctional mechanism for methanol synthesis from CO_2/H_2 is proposed (see Fig. 18) in which CO_2 is adsorbed on ZrO_2 and then undergoes stepwise hydrogenation to formate, methylenebisoxy, and methoxide species, with atomic hydrogen being supplied by spillover from Cu. The final step in this sequence is the hydrolysis of the methoxide groups on ZrO_2 via reaction with water produced as a co-product of methanol synthesis and the reverse-water–gas-shift reaction. The latter reaction is thought to occur exclusively on Cu and is not enhanced significantly by the presence of ZrO_2.

ACKNOWLEDGMENTS

The authors acknowledge Hee-Chul Woo and Johan Agrell for their assistance with these studies. This work was supported by the Director, Office of Basic Energy Sciences, Chemical Sciences Division of the U.S. Department of Energy under Contract DE-AC03-76SF00098.

REFERENCES

1. Chinchen, G. C., Waugh, K. C., and Whan, D. A., *Appl. Catal.* **25**, 101 (1986).
2. Pan, W. X., Cao, R., Roberts, D. L., and Griffin, G. L., *J. Catal.* **114**, 440 (1988).
3. Klier, K., *Adv. Catal.* **31**, 243 (1982).
4. Bartley, G. J. J., and Burch, R., *Appl. Catal.* **43**, 141 (1988).
5. Robinson, W. R. A. M., and Mol, J. C., *Appl. Catal.* **44**, 165 (1988).
6. Denise, B., and Sneeden, R. P. A., *Appl. Catal.* **28**, 235 (1986).
7. Chen, H. W., White, J. M., and Ekerdt, J. G., *J. Catal.* **99**, 293 (1986).
8. Amenomiya, Y., *Appl. Catal.* **30**, 57 (1987).
9. Denise, B., Sneeden, R. P. A., Beguin, B., and Cherifi, O., *Appl. Catal.* **30**, 353 (1987).

10. Koeppel, R. A., Baiker, A., Schild, C., and Wokaun, A., *in* "Preparation of Catalysts V," Stud. Surf. Sci. Catal. (G. Poncelet, P. A. Jacobs, P. Grange, and B. Delmon, Eds.), Vol. 63, p. 59. Elsevier, Amsterdam, 1991.
11. Kanoun, N., Astier, M. P., and Pajonk, G. M., *Catal. Lett.* **15**, 231 (1992).
12. Koeppel, R. A., Baiker, A., and Wokaun, A., *Appl. Catal. A* **84**, 77 (1992).
13. Sun, Y., and Sermon, P. A., *J. Chem. Soc., Chem. Commun.*, 1242 (1993).
14. Nitta, Y., Suwata, O., Ikeda, Y., Okamoto, Y., and Imanaka, T., *Catal. Lett.* **26**, 345 (1994).
15. Sun, Y., and Sermon, P. A., *Catal. Lett.* **29**, 361 (1994).
16. Fisher, I. A., Woo, H. C., and Bell, A. T., *Catal. Lett.* **44**, 11 (1997).
17. Schild, C., Wokaun, A., and Baiker, A., *J. Mol. Catal.* **63**, 243 (1990).
18. Baiker, A., Kilo, M., Maciejewski, M., Menzi, S., and Wokaun, A., *in* "New Frontiers in Catalysis, Proceedings of the 10th International Congress on Catalysis" (L. Guczi *et al.*, Eds.), p. 1257. Elsevier, Amsterdam, 1993.
19. Weigel, J., Koeppel, R. A., Baiker, A., and Wokaun, A., *Langmuir* **12**, 5319 (1996).
20. Hicks, R. F., Kellner, C. S., Savatsky, B. J., Hecker, W. C., and Bell, A. T., *J. Catal.* **71**, 216 (1981).
21. Kapeteijn, F., Marin, G. B., and Moulijn, J. A., *in* "Catalysis: An Integrated Approach to Homogeneous, Heterogeneous, and Industrial Catalysis," Studies in Surface Science and Catalysis, Vol. 79, Chap. 7. Elsevier, Amsterdam, 1993.
22. Millar, G. J., Rochester, C. H., Howe, C., and Waugh, K. C., *Mol. Phys.* **76**, 833 (1991).
23. Edwards, J. F., and Schrader, G. L., *J. Phys. Chem.* **88**, 5620 (1984).
24. Neophytides, S. G., Marchi, A. J., and Froment, G. F., *Appl. Catal. A* **86**, 45 (1992).
25. Millar, G. J., Rochester, C. H., and Waugh, K. C., *J. Chem. Soc. Faraday Trans.* **87**, 1491 (1991).
26. Clarke, D. B., Suzuki, I., and Bell, A. T., *J. Catal.* **142**, 27 (1993).
27. Bailey, S., Froment, G. F., Snoeck, J. W., and Waugh, K. C., *Catal. Lett.* **30**, 99 (1995).
28. Millar, G. J., Rochester, C. H., and Waugh, K. C., *J. Chem. Soc. Faraday Trans.* **81**, 2785 (1991).
29. Monti, D. M., Cant, N. W., Trimm, D. L., and Wainwright, M. S., *J. Catal.* **100**, 17 (1986).
30. Millar, G. J., Rochester, C. H., and Waugh, K. C., *J. Chem. Soc. Faraday Trans.* **87**, 2795 (1991).
31. Clarke, D. B., Lee, D. K., Sandoval, M. J., and Bell, A. T., *J. Catal.* **150**, 81 (1994).
32. Wovchko, E. A., Camp, J. C., Glass, J. A., and Yates, J. T., *Langmuir* **11**, 2592 (1995).
33. Fisher, I. A., and Bell, A. T., unpublished.
34. Tret'yakov, N. E., Pozdnyakov, D. V., Oranskaya, O. M., and Filimonov, V. N., *Russ. J. Phys. Chem.* **44**, 596 (1970).
35. Bianchi, D., Chafik, T., Khalfallah, M., and Teichner, S. J., *Appl. Catal. A* **112**, 57 (1994).
36. Bianchi, D., Chafik, T., Khalfallah, M., and Teichner, S. J., *Appl. Catal. A* **112**, 219 (1994).
37. Chafik, T., Bianchi, D., and Teichner, S. J., *Topics in Catal.* **2**, 103 (1995).
38. He, M. Y., and Ekerdt, J. G., *J. Catal.* **87**, 381 (1984).
39. Kondo, J., Abe, H., Sakata, Y., Maruya, K., Domen, K., and Onishi, T., *J. Chem. Soc. Faraday Trans. 1* **84**, 511 (1988).
40. Hertl, W., *Langmuir* **5**, 96 (1989).
41. Guglielminotti, E., *Langmuir* **6**, 1455 (1990).
42. Morterra, C., and Orio, L., *Mat. Chem. Phys.* **24**, 247 (1990).
43. Bianchi, D., Chafik, T., Khalfallah, M., and Teichner, S. J., *Appl. Catal. A* **123**, 89 (1995).
44. Bianchi, D., Chafik, T., Khalfallah, M., and Teichner, S. J., *Appl. Catal. A* **105**, 223 (1993).
45. He, M. Y., and Ekerdt, J. G., *J. Catal.* **90**, 17 (1984).
46. Argon, P. A., Fuller, E. L., and Holmes, H. F., *J. Colloid and Interface Sci.* **52**, 553 (1975).
47. Stuve, E. M., Madix, R. J., and Sexton, B. A., *Surf. Sci.* **119**, 279 (1982).
48. Lavalley, J. C., Lamotte, J., Busca, G., and Lorrenzelli, V., *J. Chem. Soc., Chem. Commun.*, 1006 (1985).
49. Onishi, T., Abe, H., Maruya, K., and Donnen, K., *J. Chem. Soc., Chem. Commun.*, 103 (1986).
50. Idriss, H., Hindermann, J. P., Kieffer, R., Kiennemann, A., Vallet, A., Chauvin, C., Lavalley, J. C., and Chaumette, P., *J. Mol. Catal.* **42**, 205 (1987).
51. Jackson, N. B., and Ekerdt, J. G., *J. Catal.* **101**, 90 (1986).
52. Clarke, D. B., and Bell, A. T., *J. Catal.* **154**, 314 (1995).
53. Sandoval, M. J., and Bell, A. T., *J. Catal.* **144**, 227 (1993).
54. Burch, R., Golunski, S. E., and Spencer, M. S., *J. Chem. Soc. Faraday Trans.* **86**, 2683 (1990).
55. Fujita, S., Usui, M., Ito, H., and Takezawa, N., *J. Catal.* **157**, 403 (1995).
56. Bianchi, D. Gass, J. L., Khalfallah, M., and Teichner, S. J., *Appl. Catal. A* **101**, 297 (1993).
57. Chinchen, G. C., Spencer, M. S., Waugh, K. C., and Whan, D. A., *J. Chem. Soc. Faraday Trans. 1* **83**, 2193 (1987).
58. Chinchen, G. C., and Spencer, M. S., *J. Catal.* **112**, 325 (1988).
59. Ernst, K. H., Campbell, C. T., and Moretti, G., *J. Catal.* **134**, 66 (1992).
60. Ovesen, C. V., Stoltze, P., Norskov, J. K., and Campbell, C. T., *J. Catal.* **134**, 445 (1992).
61. van Herwijnen, T., and deJong, W. A., *J. Catal.* **63**, 83 (1980).
62. Newsome, D. S., *Catal. Rev. Sci. Eng.* **21**, 275 (1980).
63. Klier, K., Young, C. W., and Nunan, J. G., *Ind. Eng. Chem. Fund.* **25**, 36 (1986).